Experimental investigation of turbulent flow through single-hole orifice placed in a pipe by means of time-resolved Particle Image Velocimetry and unsteady pressure measurements

Anantharaman, V.; Waterson, N.; Nakiboglu, G.; Persin, M; van Oudheusden, Bas

Publication date
2016

Document Version
Final published version

Published in
FIV 2016: Proceedings of the 11th International Conference on Flow-Induced Vibrations

11th International Conference on Flow-Induced Vibrations
4-6 July, The Hague, Netherlands

EXPERIMENTAL INVESTIGATION OF TURBULENT FLOW THROUGH SINGLE-HOLE ORIFICE PLACED IN A PIPE BY MEANS OF TIME-RESOLVED PARTICLE IMAGE VELOCIMETRY AND UNSTEADY PRESSURE MEASUREMENTS

Vinod Anantharaman*
ASML
Department of EC&I
Eindhoven
The Netherlands
Email: Vinod.Anantharaman@asml.com

Nicholas Waterson
Güneş Nakiboğlu
ASML
Department of EC&I
Eindhoven
The Netherlands

Mustafa Perçin
Bas van Oudheusden
Delft University of Technology (TU Delft)
Department of Aerospace Engineering
Delft
The Netherlands

ABSTRACT

The flow passing through a sharp-edged orifice is studied using two experimental techniques over a pipe Reynolds number range of 4000 to 27000. The flow separates at the orifice inlet and is accelerated through its hole in the form of a confined jet. For a given orifice, the mean reattachment length is found to remain fairly independent of the inflow Reynolds number. Velocity and pressure fluctuations attain peak values in regions lying upstream of the mean reattachment point. Under the conditions tested, the orifice jet shows a low frequency flapping motion which was observed to occur at a Strouhal number ≈ 0.02 based on the orifice jet velocity and the difference in internal diameters of the pipe and orifice.

NOMENCLATURE

d_h	Orifice hole diameter
D	Internal pipe diameter
f	Frequency
P'_{rms}	RMS Pressure fluctuations
Re_p	Pipe Reynolds number, $Re_p = \rho U_p D/\mu$
St	Strouhal number
t	Orifice plate thickness
t/d_h	Thickness to hole-diameter ratio
u	Axial velocity component
v	Radial velocity component
U_p	Mean pipe velocity
U_h	Orifice jet velocity
x	Axial direction
X_r	Mean reattachment length
y	Radial direction
β	Open-area ratio or porosity, $\beta = (d_h/D)^2$
ρ	Fluid density
μ	Dynamic viscosity

INTRODUCTION

Orifice plates or flow restrictions are key components used in industry for flow measurement and control. They find application in gas and liquid circuits of, e.g., lithography machines, nuclear power plants and aerospace propulsion systems [1–3]. They are used typically either for measuring flow-rate or to introduce a pressure drop for purposes of flow balancing [4, 5].

It is widely acknowledged in literature that the turbulent, unsteady nature of the flow through an orifice can be a source of noise and structural vibration [6, 7]. It introduces a sudden change in cross-section area in the path of the fluid. Due to conservation of mass, the fluid needs to accelerate in order to adjust to the change in geometry. Under turbulent entrance conditions, the flow separates at the sharp inlet edge and emerges in the form of a jet. As a result, the near field flow disturbances are primarily hydrodynamic in nature [8] and are dominated by the presence of the strong unsteady jet. As the adverse pressure gradient begins to relax, the separated flow reattaches at some distance downstream from the orifice following which the flow starts its recovery process back towards fully developed conditions. This study focuses on the characteristics of the separated flow downstream from the orifice.

*Address all correspondence to this author.

EXPERIMENTAL APPROACH

In order to understand the nature of this vibration source, experimental investigations were performed to analyze the time-varying flow field by means of,

1. Unsteady wall-pressure measurements, see Fig. 1

2. Time-resolved, planar, particle image velocimetry (PIV), see Fig. 2

focusing on the flow behavior downstream of the orifice under non-cavitating conditions. All tests were performed with water as the working fluid under fully-developed turbulent flow conditions. The average flow velocity (U_p) in the pipe was varied between $0.5-3.0$ m/s giving a Reynolds number range $Re_p = 4000-27000$. Several orifices were tested, with varying porosity β and thickness to hole-diameter ratio. The reader is directed to reference [9] for a detailed description of the considerations made in the above mentioned experiments.

Unsteady Pressure Measurements

A continuous flow of water, supplied by a pump, passes through a test section of internal diameter 9 *mm* in which the orifice plate is located before returning to the pump reservoir via a flow meter. Flush mounted pressure sensors are positioned upstream and downstream of the orifice. A differential pressure manometer measures the steady pressure difference between the flow inlet and outlet. Table 1 summarizes the data-acquisition conditions used during these experiments.

TABLE 1: PRESSURE MEASUREMENT SETTINGS

Property	Value
Acquisition frequency	2048 Hz
Sampling time	82 s
Sensors	S_1-S_6 PCB105C02, S_0 Kistler7261
Data acquisition	PAK MKII & PAK 5.8 software

Time-Resolved Planar Particle Image Velocimetry (PIV)

Water containing seeding particles, driven by a pump, passes through a flow meter and a settling chamber before approaching the orifice plate under fully-developed turbulent conditions. The fluid emerging from the orifice passes through a transparent glass tube of internal diameter 8.4 *mm* and wall thickness 0.3 *mm* and into an octagonal glass tank. The entire test section is submerged in water inside the octagonal tank and water from the tank is carried back to the reservoir. The measurement region is formed by the two-dimensional central longitudinal plane of the glass pipe downstream of the orifice plate. The tracer particles moving in this plane are illuminated by a light sheet produced by a high-speed laser. To extend the measurement region in the stream wise direction, two high-speed cameras are used, which are positioned on opposite sides of the tank, with a viewing direction orthogonal to both the tank wall and the laser-light sheet. The triggering of the laser illumination and image acquisition by the cameras is synchronized by a high-speed controller. Only results obtained from camera-1 are reported here as a majority of the features of the orifice jet are captured within the first three pipe diameters from the orifice exit. Table 2 summarizes the experimental settings used for the PIV measurements.

RESULTS & DISCUSSION

The measurements provide detailed insights into the flow behavior downstream of orifice plates and some of the key observations are described below. In all figures the flow direction is from left to right. Axial (streamwise) distances, x, are specified with respect to the orifice exit ($x = 0$) and the radial distances, y, are specified with respect to one side of the pipe.

Mean & Fluctuating Flow Field

Figure 3 presents contours of the mean and root-mean-square (RMS) of the axial velocity $(u(x,y))$ for a flow at $Re_p = 8350$ through a single-hole orifice of $\beta = 11\%$ and $t/d_h = 0.5$. A good degree of axial symmetry of the mean flow is observed. For the tested flow condition, the velocity of the jet reaches its peak value between $x = 0.1D$ and $0.5D$. The primary recirculation region extends until around $x = 2.6D$ with the peak reverse flow occurring at about $x = 1D$ (see Fig. 3b where only $\bar{u} < 0$ is shown). The RMS contours indicate a stable jet core surrounded by a higher-turbulent shear layer which reaches a peak turbulence intensity of 24%, around $1D$ upstream from the mean reattachment point.

Figure 4 presents the Reynolds number dependence of the mean reattachment length (X_r) normalized by the equivalent step-height $(0.5 \times (D - d_h))$ for orifices with $t/d_h = 0.5$ but having different porosities. For a given orifice geometry, it is observed that the mean reattachment-

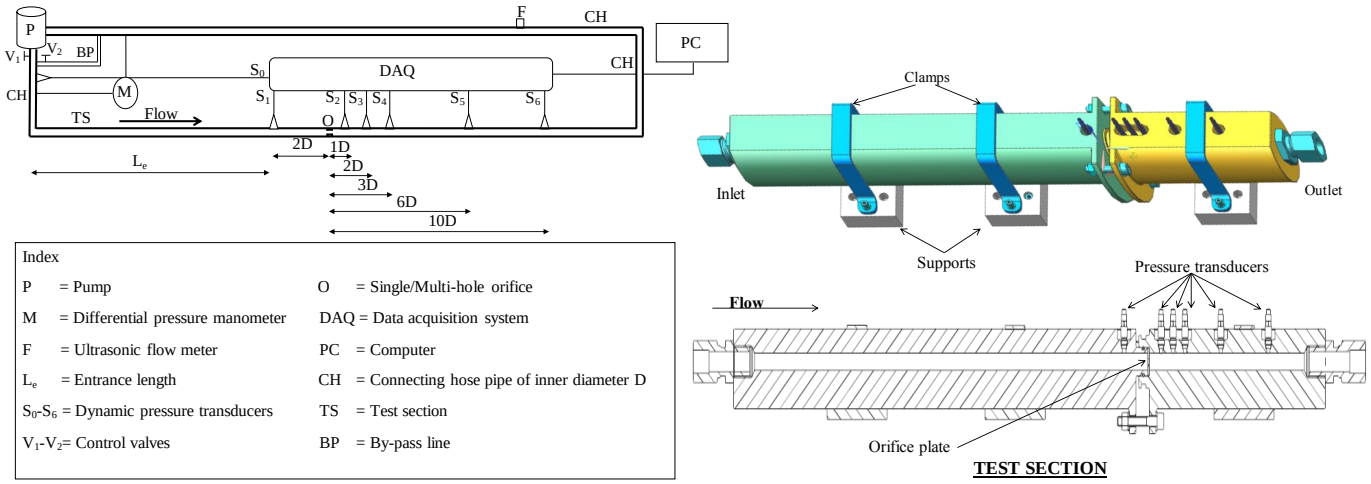

FIGURE 1: EXPERIMENTAL SETUP PRESSURE MEASUREMENTS.

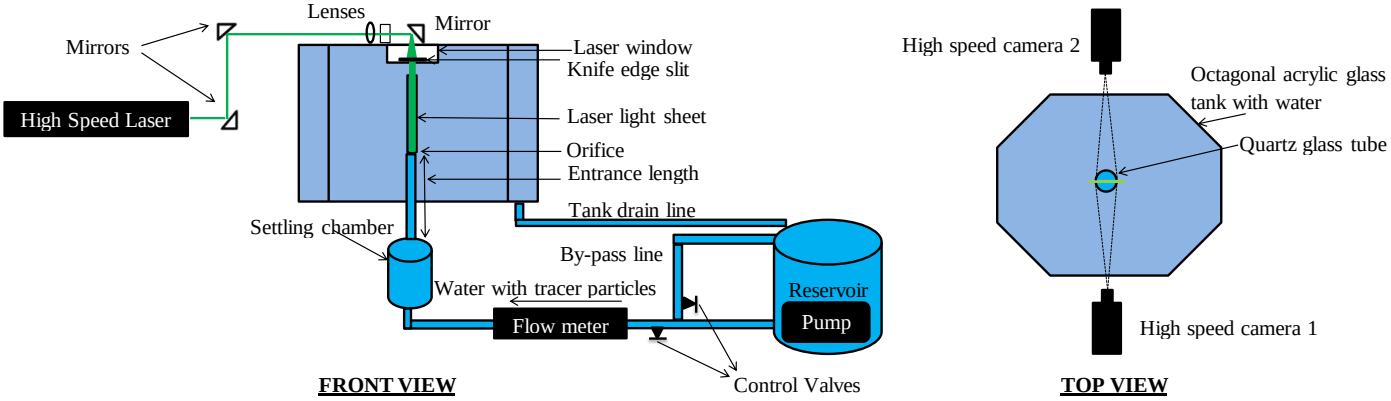

FIGURE 2: EXPERIMENTAL SETUP TIME RESOLVED PIV MEASUREMENTS.

point does not vary strongly with Reynolds number. An orifice with the lowest porosity has the largest recirculation zone surrounding the jet. As the orifice hole diameter increases, the mean reattachment point moves upstream. For the present measurement range all reattachment points lie within $6-8$ equivalent step-heights from the orifice.

The streamwise variation in the RMS of the pressure fluctuations (P'_{rms}), in the frequency range $0-1000\ Hz$, is illustrated in Fig. 5 for a range of flow speeds. P'_{rms} scales reasonably well with the mean dynamic pressure $\left(\frac{1}{2}\rho U_p^2\right)$ and attains a maximum 1-2D downstream. This location is a function of the orifice geometry. As would be expected [8], orifices with a lower porosity (higher pressure loss coefficient) produce higher pressure fluctuations.

The RMS of the pressure fluctuation levels just upstream ($-2D$) and far downstream ($6D$ & $10D$) are much lower than the near-field levels and generally mutually comparable, though the upstream values are somewhat higher for the 11% case. It would appear that the pressure disturbances observed at these locations consist mainly of the propagating (acoustic) pressure field originating from the (hydrodynamic) disturbance source close to the orifice [8, 10, 11]. It can be seen that, especially far downstream, these RMS values do not collapse completely with pipe dynamic pressure, i.e. they do not scale with U_p^2, probably as a result of increasing energy at higher frequencies, above $1000Hz$, as the flow speed increases. As a result of the acoustic field, RMS values of the fluctuating wall pressure upstream and far downstream are higher than those of undisturbed fully-developed turbulent pipe flow [12]. It should be noted that acoustic resonance can be expected in the fluid contained in the working section due to wave reflection at the hose connections [13], however the frequency of the first mode, around 1500 Hz, is outside the frequency range considered here.

TABLE 2: EXPERIMENTAL SETTINGS PIV MEASUREMENTS

Seeding	Silver coated hollow glass spheres
Mean diameter	10 μm
Concentration	15 particles/mm^3
Illumination	Litron laser
Maximum repetition rate	20 kHz
Sheet thickness	0.5 mm
Recording device	High-speed star 6 (Two)
Minimum exposure time	1 μs
Pixel pitch	20 μm
Optical arrangement	Nikon lenses
f & $f_\#$	180 mm & 5.6 respectively
Field of View	$7.4D \times 1D$
Camera-1 $(x \times y)$	(0 - $3.9D$) $\times$ (0-$1D$)
Camera-2 $(x \times y)$	($2.9D$ - $7.4D$) $\times$ (0-$1D$)
Overlap region (x)	$2.9D$ - $3.9D$
Acquisition frequency	Double frame 1.5 kHz
	Single frame 12.5 kHz
Sample size	3000 images double frame
	6000 images single frame

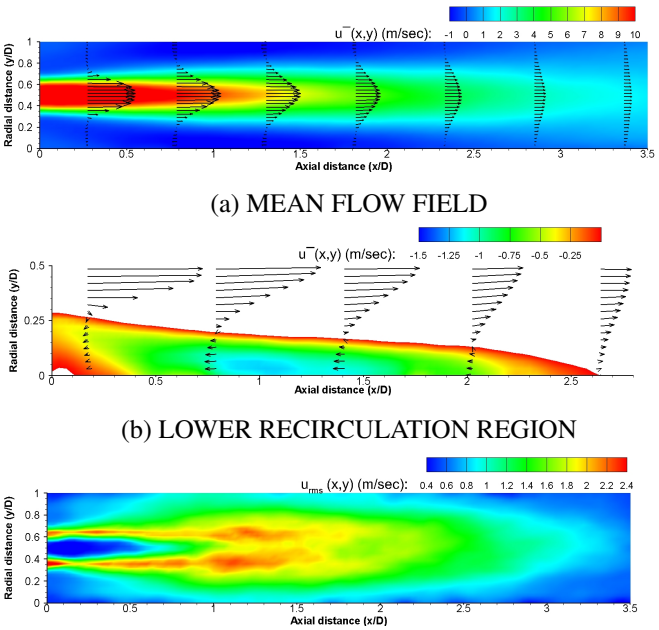

(a) MEAN FLOW FIELD

(b) LOWER RECIRCULATION REGION

(c) RMS FLOW FIELD

FIGURE 3: AXIAL VELOCITY COMPONENT OF THE FLOW FIELD.

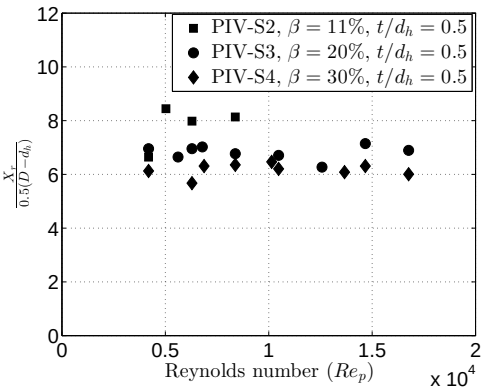

FIGURE 4: REYNOLDS NUMBER VARIATION OF NORMALIZED MEAN REATTACHMENT LENGTH

Figure 6a presents the Power Spectral Density (PSD) of the wall pressure fluctuations measured at different axial distances from the orifice exit for a flow at $Re_p = 18000$ through an orifice with $\beta = 20\%$ and $t/d_h = 0.5$. Analysis of the pressure spectra reveals the existence of a dominant frequency close to the orifice (up to $x = 1-2D$) which is observed to scale linearly with the flow velocity (see Fig. 6b) with a Strouhal number $St \approx 0.02$ based on U_h and $(D - d_h)$, in the measurement range. As observed for the RMS values, the spectra at the locations upstream ($-2D$) and far downstream ($6D$ & $10D$) are mutually comparable and distinct from the near-field spectra. It is also noticeable that they do not display the $St \approx 0.02$ peak, indicating that this does not seem to be a feature of the propagating pressure field.

Unsteady Flow Analysis

Some of the time-varying features of the orifice jet can be seen in Fig. 7, which corresponds to a flow at $Re_p = 8383$ through an orifice with $\beta = 20\%$ and $t/d_h = 0.5$. Each flow-field is at a given time instant t_i, arranged chronologically as $\{t_1 t_2 \cdots t_8\}$, with a difference of 20 images between consecutive images. Vector fields are computed using sliding sum-of-correlation on data sampled at 12500 Hz. The orifice jet length is observed to vary in time. It appears that the shear layer grows (extends) till a certain extent after which a portion of the fluid breaks off upon which the jet length decreases again. Another noticeable feature is the constriction of the jet. These im-

ages also illustrate the lateral motion of the jet with respect to the pipe centerline, which appears as a flapping motion in the time series.

The unsteady organization of the velocity field is further analysed using Proper Orthogonal Decomposition (POD) [14] to identify coherent structures (eigenmodes) present in the flow [15, 16]. Physically, each eigenmode can be considered as capturing dominant characteristics

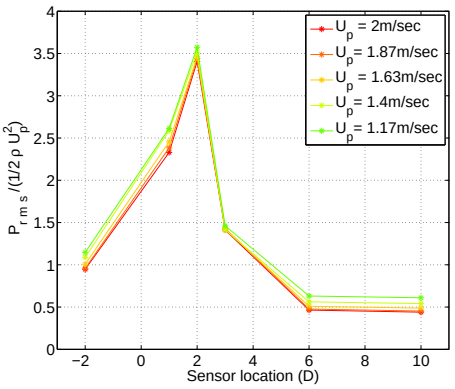

(a) $\beta = 11\%$ $t/d_h = 0.5$

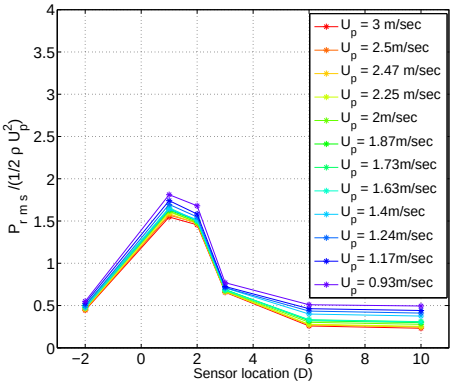

(b) $\beta = 20\%$ $t/d_h = 0.5$

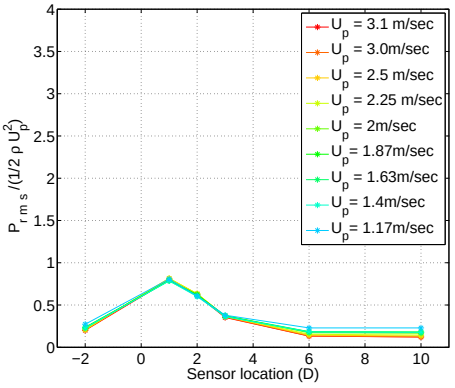

(c) $\beta = 30\%$ $t/d_h = 0.5$

FIGURE 5: AXIAL VARIATION OF $P'_{rms}/(\frac{1}{2}\rho U_p^2)$

.

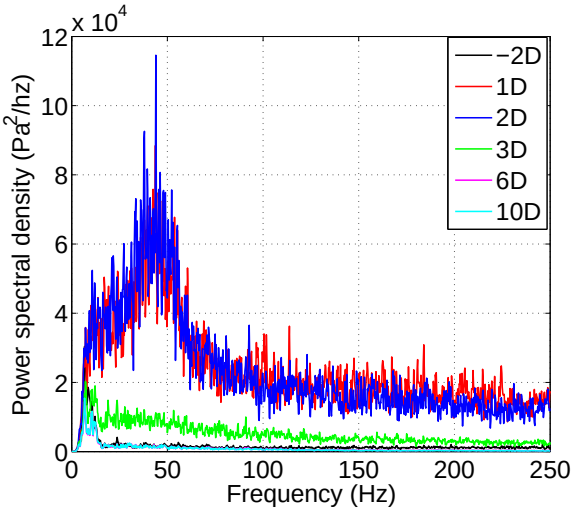

(a) PSD PRESSURE FLUCTUATIONS ($Re_p = 18000$)

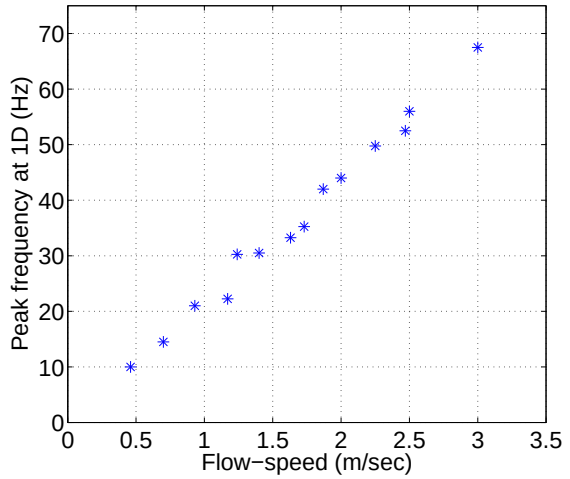

(b) PEAK FREQUENCY VARIATION WITH FLOW SPEED

FIGURE 6: RESULTS FROM PRESSURE MEASUREMENTS ($\beta = 20\%$ and $t/d_h = 0.5$)

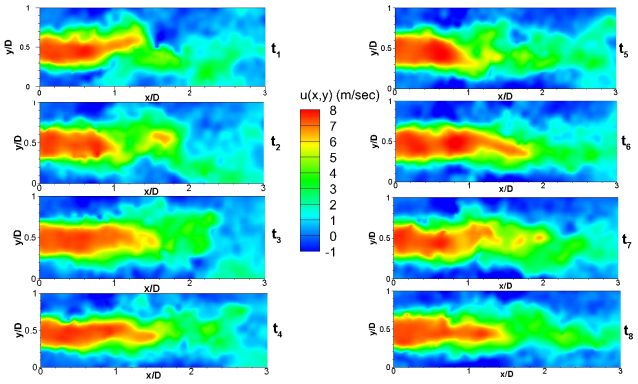

FIGURE 7: TIME SERIES ILLUSTRATING THE UNSTEADY FLOW FIELD.

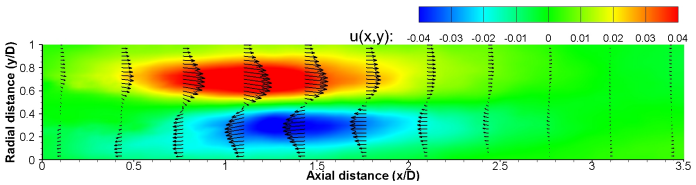

(a) FIRST SPATIAL POD MODE

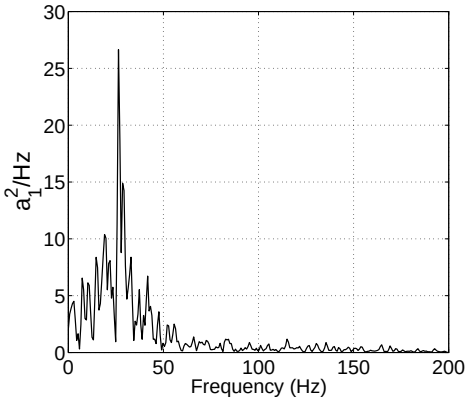

(b) SPECTRUM OF THE FIRST TEMPORAL MODE.

FIGURE 8: POD ANALYSIS OF PIV DATA

of the flow and should not be misinterpreted as instantaneous physical structures [17]. The POD coefficients contain temporal information related to the spatial structures and gives access to the frequencies dominant in each mode, provided the snapshots represent a time-resolved sequence. In general, more than a single frequency can be associated with each structure.

Figure 8 presents the first spatial POD mode and the spectrum of its corresponding temporal mode computed using a data set of 1000 snapshots with each snapshot separated by $3/1500$ s for a flow at $Re_p = 8383$ through an orifice with $\beta = 20\%$ and $t/d_h = 0.5$. The spectra of the wall-pressure fluctuation data were compared against velocity field spectra extracted from the temporal mode. The dominant peak in the spectrum agrees well with the pressure data, while the spatial distribution of the POD mode indicates that the primary instability of the orifice jet is a low-frequency flapping motion sustained by the surrounding large recirculation regions.

Figure 9 presents the variation of the Strouhal number ($St = f \times L/U_h$) corresponding to the low-frequency peak observed in the wall-pressure measurements as a function of pipe Reynolds-number (Re_p). Colours differentiate orifice geometries while different symbols distinguish length scales (L) used for defining the Strouhal number.

For the geometries of the sharp-edged orifices that were investigated (with $t/d_h = 0.5$), the best collapse of

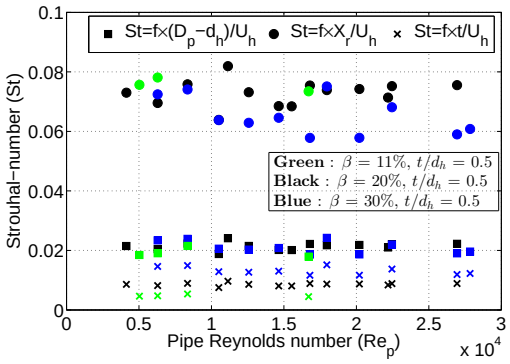

FIGURE 9: REYNOLDS NUMBER VARIATION OF THE NON DIMENSIONAL FLAPPING FREQUENCY

the data is achieved when taking the reference length as the pipe to orifice diameter difference $(D - d_h)$, in which case a Strouhal number ≈ 0.02 is obtained.

CONCLUSION

1. Turbulent flow of water through a sharp-edged, thin, single-hole orifice contained in a pipe results in a strong unsteady jet surrounded by large recirculation regions whose extent is a function of the orifice geometry.

2. The RMS level of the downstream pressure fluctuations was found to scale quadratically with the incoming flow speed with peak fluctuation levels occurring within 0 to $2D$ for the present measurement conditions. A comparison of PIV and pressure measurements showed that the peak velocity and pressure fluctuations occur in the upstream vicinity of the mean reattachment point.

3. The mean reattachment length, X_r, was observed to be rather insensitive to Reynolds number and was within 6 to 8 equivalent step heights $((D - d_h)/2)$ for the orifices tested. In that sense, the flow is analogous to turbulent flow past a planar backward-facing step or axisymmetric pipe expansion.

4. Both velocity and pressure measurements show indications of a dominant low frequency with a Strouhal number of ≈ 0.02, based on on the orifice jet velocity U_h and $(D - d_h)$, or 0.075, based on the mean reattachment length. This frequency is observed in the downstream vicinity of the orifice and doesn't seem to propagate.

REFERENCES

[1] Ahuja, V., Hosangadi, A., Hitt, M., and Lineberry, D., 2013. "Numerical Simulations of Instabilities in Single-Hole Orifice Elements". In 49^{th} AIAA/ASME/SAE/ASEE Joint Propulsion Conference.

[2] Haimin, W., Shujuan, X., Qingyi, S., Caimin, Z., Hao, L., and Eryun, C., 2013. "Experiment study on pressure drop of a multistage letdownorifice tube". *Nuclear Engineering and Design,* ***265***, pp. 633–638.

[3] Howes, B., and Greenfield, D., 2002. "Guidelines in pulsation studies for reciprocating compressors". In 4^{th} International Pipeline Conference.

[4] Idelchik, I., 2008. *Handbook of hydraulic resistance*, 4^{th} ed. Begell House.

[5] Miller, D., 1990. *Internal flow systems*, 2^{nd} ed. Miller Innovations.

[6] Agarwal, N., 1994. "The sound field in fully developed turbulent pipe flow due to internal flow separation, part 1: wall-pressure fluctuations". *Journal of Sound and Vibration,* ***169***, pp. 89–109.

[7] Agarwal, N., 1994. "The sound field in fully developed turbulent pipe flow due to internal flow separation, part 2: modal amplitude and cut-off frequencies". *Journal of Sound and Vibration,* ***175***, pp. 65–76.

[8] Moussou, P., 2006. "An attempt to scale the vibrations of water pipes". *Journal of pressure vessel technology,* ***128***, pp. 670–676.

[9] Anantharaman, V., 2014. "Characteristics of flow through orifices in pipes: an experimental investigation". Master's thesis, TU Delft.

[10] Testud, P., Aurégan, Y., Moussou, P., and Hirschberg, A., 2009. "The whistling potentiality of an orifice in a confined flow using an energetic criterion". *Journal of Sound and Vibration,* ***325***, pp. 769–780.

[11] Lacombe, R., Föller, S., Jasor, G., Polifke, W., Aurégan, Y., and Moussou, P., 2013. "Identification of aero-acoustic scattering matrices from large eddy simulation: Application to whistling orifices in duct". *Journal of Sound and Vibration*.

[12] Norton, M., and Bull, M., 1984. "Mechanism of the generation of external acoustic radiation from pipes due to internal flow disturbances.". *Journal of Sound and Vibration,* ***94***, pp. 105–146.

[13] Moonen, C., Waterson, N., Kemper, N., and Smeulders, D., 2016. "Experimental study of resonance in water circuit with mixed rigid ducts and flexible hosing". In 11^{th} International Conference on Flow-Induced Vibrations.

[14] Sirovich, L., 1987. "Turbulence and the dynamics of coherent structures. Part I: Coherent structures.". *Quarterly of Applied Mathematics,* ***45***, pp. 561–571.

[15] Meyer, K., Pederson, J. M., and Özcan, O., 2007. "A turbulent jet in crossflow analysed with proper orthogonal decomposition". *Journal of Fluid Mechanics,* ***583***, pp. 197–227.

[16] Semeraro, O., Bellani, G., and Lundell, F., 2012. "Analysis of time-resolved PIV measurements of a confined turbulent jet using POD and Koopman modes". *Experiments in Fluids,* ***53***, pp. 1203–1220.

[17] Van Oudheusden, B. W., Scarano, F., van Hinsberg, N. P., and Watt, D. W., 2005. "Phase-resolved characterization of vortex shedding in the near wake of a square-section cylinder at incidence". *Experiments in Fluids,* ***39***, pp. 86–98.